energies

MDPI

Article

A Mathematical Approach of Voltage Sag Analysis Incorporating Bivariate Probability Distribution in a Meshed System

Jagannath Patra and Nitai Pal *

Department of Electrical Engineering, Indian Institute of Technology (Indian School of Mines), Dhanbad 826004, India
* Correspondence: nitai@iitism.ac.in; Tel.: +91-9471154739

Abstract: In this paper, different mathematical expressions are derived to compute the residual magnitude of voltage caused by faults along the line and on the bus. Symmetrical and unsymmetrical faults are taken into consideration, and the consequences of the various fault distributions are considered. A new way of assessing a sag is proposed that incorporates the method of fault position and mathematical expression based on sequence currents and voltages. The fault impedance is introduced to obtain a better result. A fast and efficient load flow analysis technique produces quick computational results. In addition, the sag analysis is performed using the bivariate joint discrete probability distribution method that gives a clear idea about the probability of occurrence of sag in a meshed network. The suggested approach is applied in the IEEE 39-bus system and with an existing real-time electrical power distribution system in India.

Keywords: fault position method; symmetrical and unsymmetrical fault; voltage sag assessment; mathematical approach; bivariate joint probability distribution

Citation: Patra, J.; Pal, N. A Mathematical Approach of Voltage Sag Analysis Incorporating Bivariate Probability Distribution in a Meshed System. *Energies* **2022**, *15*, 7592. https://doi.org/10.3390/en15207592

Academic Editors: Juan-José González de la Rosa, Sara Sulis and Olivia Florencias-Oliveros

Received: 15 August 2022
Accepted: 5 October 2022
Published: 14 October 2022

1. Introduction

Among the different types of power quality problems, voltage sags are the most important. Voltage sags are reductions in the RMS value of voltage for a short time. The main reasons for sags are short-circuiting faults and the starting of large motors [1–4], characterized by their magnitude of voltage and duration. The magnitude lies between 10% and 90%, and the sag duration lasts for between 10 ms and 1 min [5]. The magnitude of sag is the residual voltage during the occurrence of an event. It depends upon various parameters, namely, the fault types, the location of faults, the transformer connection, the voltage before the fault, and the fault impedance. The sag source location is the most important parameter, which directly affects the voltage for the bus [6–8]. Sag duration is the duration for which the sag lasts or throughout which the root-mean-square value of voltage persists at a lower magnitude than the granted nominal voltage. It is associated with the time required to clear the relevant fault. Consequently, the sag interval can be determined by analyzing different characteristics of the electrical protective equipment, such as fuses, circuit breakers, and overcurrent relays.

Voltage sags cause critical issues as new manufacturing and control industries have progressively been developed that incorporate sensitive types of equipment whose entire process may stop due to severe voltage sag [9–12]. The disturbance in an industrial or technical approach is due to supply interruption or sag, leading to considerable costs to its operation [13]. Production processes have a price, extending up to millions of dollars due to a single disturbance [14–16]. Sags or different power quality (PQ) issues should be inspected as a concord disturbance between the power supply and the sensitive load at the PCC (point of common coupling). This type of method needs to explain the predicted sag performance, as well as provide an applicable explanation of a given load's sensitivity to voltage sag in a network at the PCC. Therefore, it is necessary to know the performance of the power system. At the given site, the performance of the power system can be analyzed in terms of its characteristics and the predicted frequency of sags. The power system's performance can be determined by stochastic prediction or by monitoring the supply. A monitoring method is an approach to collecting information about a system's performance. However, a long monitoring duration is essential for high accuracy. The alternative way to get information about voltage sags is the process of stochastic prediction [17–19]. Two approaches are available to analyze the stochastic forecasting of voltage sags. These are the methods of fault position and critical distance. The easier way of forecasting sags can be done by the process of critical distance, which is explained based on the theory of the voltage divider rule. Commonly, this method of assessment is used in the radial system. In the method of fault position, several probable fault positions are simulated simultaneously using the typical theory of short-circuiting [2]. Each simulated fault position is a fault in a specific portion of the considered system. The possibility of short-circuit faults is linked with the fault rate of the buses and lines. Meanwhile, the voltage due to faults observed on any bus is then analytically evaluated to obtain the characteristics of the sags of the network [20].

The work is extended with a comparison to reference [3]. In the research article, the fault impedance was not considered, and it was followed by the existing typical load flow analysis technique. In the presented article, fault impedance is introduced, due to which more voltage sags occur, which can be treated better so that the industrial consumer will be prepared for this type of contingency. This article uses a fast and efficient load flow analysis technique to produce fast results. Computational performance is enhanced. Apart from that, the sag analysis is done by using the bivariate joint discrete probability distribution method that uses a joint probability mass function, which gives a clear idea about the probability of the occurrence of sag in a meshed network. These three things: (a) introduction of fault impedance, (b) application of a fast and efficient load flow analysis technique, and (c) use of bivariate joint discrete probability distribution, claim the novelty of the proposed article. The proposed method is applied to the IEEE 39-bus system and an existing distribution system in India.

2. Fault Position Approach and Methods

The method of fault position for calculating the frequency of sags was suggested by Bollen [2]. It is a simple technique used to compute the probable frequency of voltage sags in a meshed system. This method is robust and overcomes the shortcomings of the critical distance method. The accuracy of the outcomes can be enhanced by increasing the frequency of fault positions and splitting the whole system into small parts; the short circuit inside one miniature part leads to voltage sags with identical features.

In the circuit model of the considered network, each small part is treated as a one-fault position. The frequency of short circuits is determined for all the fault positions. By using the electrical equivalent model of the considered network, the voltage sag features are determined for all the fault positions. The outcomes from the two preceding steps (frequency of occurrence and sag characteristics) are assembled to find data about the frequency of sags with features within a certain definite extent stochastically. Figure 1 represents part of a power system. It is a 100-km line with eight fault positions representing a short-circuit fault.

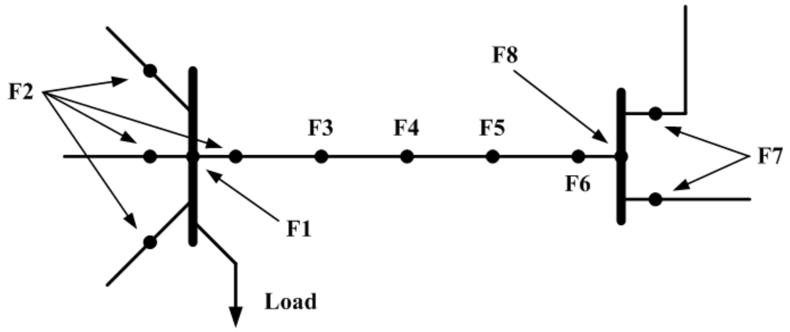

Figure 1. Part of a network with fault positions.

The selection of the different fault positions is based on the characteristics of sag, which are considered for the study of interest. Sag duration and magnitude are considered in this example. Fault positions F1 (indicating faults on the bus bar in the substation) and F2 (faults nearer to the bus bar) lead to the same magnitude of sag, but their fault-clearing times are different. Hence, two fault positions have been selected. The fault positions (F2, F3, F4, and F5) along the line have different magnitudes of sag but similar fault-clearing times. Fault positions F6, F7, and F8 result in different durations of sag but the same magnitude. For all fault positions, magnitude, duration, and frequency are determined. It is noted that all the fault positions need not be an equal fraction of the distance along the line. The length (x) between fault positions for any lines originating from the substation is given by Equation (1) [2].

$$x = \frac{V_{nm}}{Z\sqrt{3}\, I_{flt}}\left(\frac{V_{sag}}{1 - V_{sag}}\right) \tag{1}$$

where V_{nm} is the nominal voltage (phase to phase), I_{flt} is the terminal fault current in the feeder, Z is the impedance of feeder per unit length, and V_{sag} is the magnitude of the sag. Pre-fault voltage is assumed as a unity per unit, and the load current is ignored for this mathematical expression of Equation (1).

3. Suggested Mathematical Approach

This study focused on sag that occurred due to symmetrical and unsymmetrical faults. The mathematical equation for the remaining phase voltages for symmetrical and unsymmetrical faults observed along a random line is obtained to get the magnitude of the dip.

3.1. Faults at the System Buses

Figure 2 describes various types of faults in the power system. Sags due to a fault at any usual bus ϕ of the system and the voltages in terms of unsymmetrical sequence components at bus Ψ are expressed in Equations (2)–(4) [3,21,22]:

$$V_{\Psi}^{0} = 0 - Z_{\Psi\phi}^{0} I_{\phi}^{0} \tag{2}$$

$$V_{\Psi}^{1} = V_{\Psi}^{1Prf} - Z_{\Psi\phi}^{1} I_{\phi}^{1} \tag{3}$$

$$V_{\Psi}^{2} = 0 - Z_{\Psi\phi}^{2} I_{\phi}^{2} \tag{4}$$

Equations (2)–(4) can be expressed in terms of vector sequence components as shown in Equation (5).

$$\overline{V_{\Psi}^{012}} = \overline{V_{\Psi}^{012Prf}} - \left[Z_{\Psi\phi}^{012}\right] \overline{I_{\phi}^{012}} \tag{5}$$

where $\overline{V_{\Psi}^{012}} = \begin{bmatrix} V_{\Psi}^{0} \\ V_{\Psi}^{1} \\ V_{\Psi}^{2} \end{bmatrix}$ and the terms V_{Ψ}^{1}, V_{Ψ}^{2}, and V_{Ψ}^{0} are the positive, negative, and zero vectors of sequence voltage at the usual bus bar Ψ, correspondingly.

$\overline{V_{\Psi}^{012Prf}} = \begin{bmatrix} V_{\Psi}^{0Prf} \\ V_{\Psi}^{1Prf} \\ V_{\Psi}^{2Prf} \end{bmatrix}$ where V_{Ψ}^{1Prf}, V_{Ψ}^{2Prf}, and V_{Ψ}^{0Prf} are the positive, negative and zero sequence vectors of pre-fault voltage, correspondingly.

$Z_{\Psi\phi}^{012} = \begin{bmatrix} Z_{\Psi\phi}^{0} & 0 & 0 \\ 0 & Z_{\Psi\phi}^{1} & 0 \\ 0 & 0 & Z_{\Psi\phi}^{2} \end{bmatrix}$ where $Z_{\Psi\phi}^{0}$, $Z_{\Psi\phi}^{2}$, and $Z_{\Psi\phi}^{0}$ are the transfer sequence impedance of the line that connects bus Ψ and ϕ. $\overline{I_{\phi}^{012}} = \begin{bmatrix} I_{\Psi}^{0} \\ I_{\Psi}^{1} \\ I_{\Psi}^{2} \end{bmatrix}$ where the term I_{Ψ}^{1}, I_{Ψ}^{2}, and I_{Ψ}^{0} are the positive, negative and zero sequence fault current vectors at bus Ψ, respectively. Equation (5) applies to the bus bar fault of the network. When there are occurrences of faults along any arbitrary line of the network, the mathematical expressions must be continued.

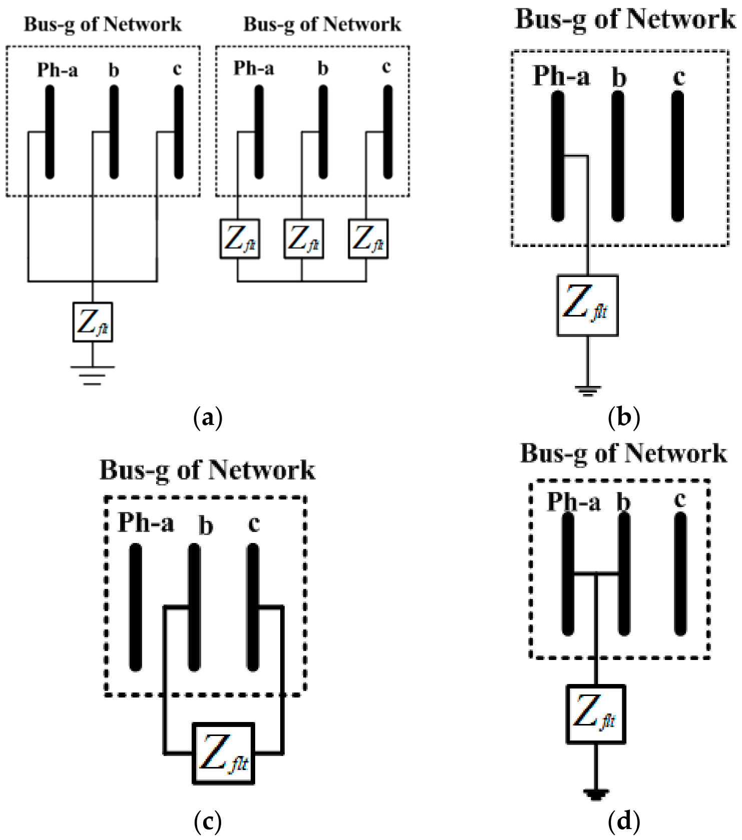

Figure 2. Occurrence of faults at bus g named as (**a**) Symmetrical fault; (**b**) Single line to ground fault at phase-a; (**c**) Line-to-line fault at phase-b and phase-c; (**d**) Double line to ground fault at phase-a and phase-b.

3.2. Voltage Sag Due to a Line Fault

We will now focus on a position of fault g that moves throughout a considered line, joining buses B and C. As shown in Figure 3, the location of g is where the occurrence of a fault is determined by the use of an introduced parametric quantity, δ. The value of parametric quantity δ lies between 0 to 1 concerning the movement of the location of the fault from bus B to C.

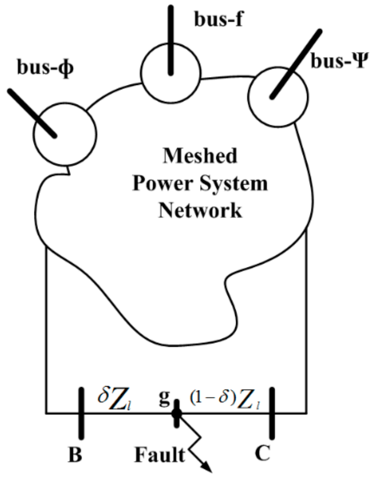

Figure 3. Short-circuit faults in line B-C and perceptive P-Q bus ψ.

Therefore, δ can be defined as shown in Equation (6) [3,18]

$$\delta = \left(D_{Bg}/D_{BC}\right) ;\ 0 \leq \delta \leq 1 \tag{6}$$

where D_{Bg} indicates the distance between fault point g and bus B, and D_{BC} represents the distance between fault point bus B and bus C.

The driving point and transfer impedances of three sequence circuits can be represented employing positive (Z^1), negative (Z^2), and zero (Z^0) sequence impedances and parametric quantity δ. The sequence transfer impedances within the fault position g and perceptive P-Q bus ψ can be mathematically expressed as shown in Equations (7)–(9) [3,16]:

$$Z^0_{\Psi g} = \delta Z^0_{\Psi C} + (1-\delta)\ Z^0_{\Psi B} \tag{7}$$

$$Z^1_{\Psi g} = \delta Z^1_{\Psi C} + (1-\delta)\ Z^1_{\Psi B} \tag{8}$$

$$Z^2_{\Psi g} = \delta Z^2_{\Psi C} + (1-\delta)\ Z^2_{\Psi B} \tag{9}$$

where $Z^0_{\Psi B}$, $Z^1_{\Psi B}$, and $Z^2_{\Psi B}$ are the sequence transfer impedances related to buses Ψ and B, and $Z^0_{\Psi C}$, $Z^1_{\Psi C}$, and $Z^2_{\Psi C}$ are the sequence transfer impedances related to buses Ψ and C. At the location of fault g, the sequence driving point impedance can be stated mathematically in Equation (10):

$$\begin{bmatrix} Z^0_{gg} \\ Z^1_{gg} \\ Z^2_{gg} \end{bmatrix} = \begin{bmatrix} (1-2\delta+\delta^2)\ 2\delta(1-\delta)\ \delta^2\ \delta(1-\delta) \\ (1-2\delta+\delta^2)\ 2\delta(1-\delta)\ \delta^2\ \delta(1-\delta) \\ (1-2\delta+\delta^2)\ 2\delta(1-\delta)\ \delta^2\ \delta(1-\delta) \end{bmatrix} \begin{bmatrix} Z^0_{BB}\ Z^1_{BB}\ Z^2_{BB} \\ Z^0_{BG}\ Z^1_{BG}\ Z^2_{BG} \\ Z^0_{GG}\ Z^1_{GG}\ Z^2_{GG} \\ Z^0_{l}\ Z^1_{1}\ Z^2_{1} \end{bmatrix} \tag{10}$$

where Z^{012}_{BB} and Z^{012}_{CC} are the sequence driving point impedances and Z^{012}_{BC} are the sequence transfer impedances at the shown buses B and C, respectively, and Z^{012}_{l} are the sequence impedances of the line between buses B and C. The voltage before the fault at the position of fault g can furthermore be stated mathematically in Equation (11):

$$V_g = (1-\delta)V_B + \delta V_C \tag{11}$$

where V_B and V_C are the pre-fault voltages at buses B and C, correspondingly.

3.3. Symmetrical Fault (Three-Phase Fault)

Zero and negative sequences are not considered here. When this balanced fault occurred as shown in Figure 2 at the bus g, then the voltage remains in a bus Ψ is given in Equation (12) [3,23]

$$V_{\Psi}^{flt} = V_{\Psi}(0) - \frac{Z_{\Psi g}^{1}}{Z_{gg}^{1}} V_{g}(0) \tag{12}$$

where $Z_{\Psi g}^{1}$ is the positive sequence impedance between bus g and Ψ, and Z_{gg}^{1} is the sequence driving point impedance associated with bus g. $V_{\Psi}(0)$ and $V_{g}(0)$ are the voltages before the fault in bus ψ and g. V_{Ψ}^{flt} refers to the voltage remains in bus ψ after the symmetrical fault at bus g.

3.4. Single Line to Ground Fault (SLGF)

The mathematical expression of voltage remains in phase-a, b, and c, respectively, of the bus ψ as a result of the occurrence of SLGF at bus g, which is given in Equations (13)–(15) [3,18,23].

$$V_{a,\Psi}^{flt} = V_{\Psi}^{1}(0) - V_{g}(0)\left[\frac{Z_{\Psi g}^{1} + Z_{\Psi g}^{2} + Z_{\Psi g}^{0}}{3Z_{flt} + Z_{gg}^{1} + Z_{gg}^{2} + Z_{gg}^{0}}\right] \tag{13}$$

$$V_{b,\Psi}^{flt} = V_{\Psi}^{1}(0) - V_{g}(0)\left[\frac{\alpha^{2} Z_{\Psi g}^{1} + \alpha Z_{\Psi g}^{2} + Z_{\Psi g}^{0}}{3Z_{flt} + Z_{gg}^{1} + Z_{gg}^{2} + Z_{gg}^{0}}\right] \tag{14}$$

$$V_{c,\Psi}^{flt} = V_{\Psi}^{1}(0) - V_{g}(0)\left[\frac{\alpha Z_{\Psi g}^{1} + \alpha^{2} Z_{\Psi g}^{2} + Z_{\Psi g}^{0}}{3Z_{flt} + Z_{gg}^{1} + Z_{gg}^{2} + Z_{gg}^{0}}\right] \tag{15}$$

where $Z_{\Psi g}^{1}$, $Z_{\Psi g}^{2}$, and $Z_{\Psi g}^{0}$ are the positive, negative, and zero-sequence impedances between buses g and Ψ, respectively. $V_{a,\Psi}^{flt}$, $V_{b,\Psi}^{flt}$, and $V_{c,\Psi}^{flt}$ are the voltage remains after the SLGF in phase-a, b, and c respectively of the bus Ψ. Z_{gg}^{0}, Z_{gg}^{1}, and Z_{gg}^{2} are the sequence driving point impedances of g axis of associated bus impedance matrix. And $V_{\Psi}^{1}(0)$ is the positive sequence voltage at bus Ψ before the fault and Z_{flt} is the fault impedance respectively.

3.5. Line to Line Fault (LLF)

The mathematical expression of voltage remains in phase-a, b, and c respectively of the bus Ψ as a result of the occurrence of LLF at bus-g is given in Equations (16)–(18) [3,18,23].

$$V_{a,\Psi}^{flt} = V_{\Psi}^{1}(0) - V_{g}(0)\left[\frac{Z_{\Psi g}^{1} - Z_{\Psi g}^{2}}{Z_{flt} + Z_{gg}^{1} + Z_{gg}^{2}}\right] \tag{16}$$

$$V_{b,\Psi}^{flt} = \alpha^{2} V_{\Psi}^{1}(0) - V_{g}(0)\left[\frac{\alpha^{2} Z_{\Psi g}^{1} - \alpha Z_{\Psi g}^{2}}{Z_{flt} + Z_{gg}^{1} + Z_{gg}^{2}}\right] \tag{17}$$

$$V_{c,\Psi}^{flt} = \alpha V_{\Psi}^{1}(0) - V_{g}(0)\left[\frac{\alpha Z_{\Psi g}^{1} - \alpha^{2} Z_{\Psi g}^{2}}{Z_{flt} + Z_{gg}^{1} + Z_{gg}^{2}}\right] \tag{18}$$

where $Z_{\Psi g}^{1}$, $Z_{\Psi g}^{2}$, and $Z_{\Psi g}^{0}$ are the positive, negative, and zero sequence impedances between bus g and Ψ respectively. $V_{a,\Psi}^{flt}$, $V_{b,\Psi}^{flt}$, and $V_{c,\Psi}^{flt}$ are the voltage remains after the LLF in phase-a, b, and c, correspondingly, of the bus Ψ.

3.6. Double Line to Ground Fault (DLGF)

The mathematical expression of positive, negative, and zero-sequence of current that occurred due to LLF as shown in Figure 2 and expressed in Equations (19)–(21) [3,18,23].

$$I_g^1 = V_g(0) / \left[Z_{gg}^1 + \frac{Z_{gg}^2 \left(Z_{gg}^0 + 3Z_{flt} \right)}{Z_{gg}^2 + Z_{gg}^0 + 3Z_{flt}} \right] \tag{19}$$

$$I_g^2 = -\frac{V_g(0) - Z_{gg}^1 I_g^1}{Z_{gg}^2} \tag{20}$$

$$I_g^0 = \frac{V_g(0) - Z_{gg}^1 I_g^1}{Z_{gg}^0 + 3Z_{flt}} \tag{21}$$

where I_g^1, I_g^2, and I_g^0 are the positive, negative, and zero-sequence currents, correspondingly, due to DLGF. Z_{gg}^1, Z_{gg}^2, and Z_{gg}^0 are the sequence driving point impedances of the g axis of the associated bus impedance matrix, and Z_{flt} is the fault impedance. Simultaneously, the sequence and phase voltage remains in different phases at the bus Ψ as a result of the occurrence of the DLGF at bus g are expressed Equations (25)–(27).

$$V_\Psi^1(flt) = V_\Psi^1(0) - Z_{\Psi g}^1 I_g^1 \tag{22}$$

$$V_\Psi^2(flt) = 0 - Z_{\Psi g}^2 I_g^2 \tag{23}$$

$$V_\Psi^0(flt) = 0 - Z_{\Psi g}^0 I_g^0 \tag{24}$$

$$V_{a,\Psi}^{flt} = V_\Psi^0(flt) + V_\Psi^1(flt) + V_\Psi^2(flt) \tag{25}$$

$$V_{b,\Psi}^{flt} = V_\Psi^0(flt) + \alpha^2 V_\Psi^1(flt) + \alpha V_\Psi^2(flt) \tag{26}$$

$$V_{c,\Psi}^{flt} = V_\Psi^0(flt) + \alpha V_\Psi^1(flt) + \alpha^2 V_\Psi^2(flt) \tag{27}$$

where $Z_{\Psi g}^1$, $Z_{\Psi g}^2$, and $Z_{\Psi g}^0$ are the positive-, negative-, and zero-sequence impedances between buses g and Ψ, respectively. $V_\Psi^0(flt)$, $V_\Psi^1(flt)$, and $V_\Psi^2(flt)$ are the zero-, positive-, and negative-sequence currents, respectively, due to DLGF. $V_{a,\Psi}^{flt}$, $V_{b,\Psi}^{flt}$, and $V_{c,\Psi}^{flt}$ are the voltage remains after the DLGF in phase-a, b, and c, respectively, of bus ψ.

4. Sag Analysis Using Bivariate Discrete Probability Distribution

For the analysis, B and C consecutive buses were chosen in Figure 3. The fault may occur between these two points, B and C. Due to this, line fault voltage sag occurs in different buses. Let '*W*' be the sag magnitude range parameter. For the analysis, the magnitude ranges are categorized into a 0.1 p.u. gap, and the discrete sag frequency is allocated in the associated range. Thus, it is taken as one discrete random variable. Symbol '*K*' is taken as a fault parameter, which is also a discrete random variable whose discrete value varies from 1 to 4 for the different types of faults (symmetrical, SLGF, LLF, and DLGF).

The joint probability mass function of these two continuous random variables is shown in Equations (28)–(32) [24].

$$P_{prob}(W = w_i,\ K = k_J) = (P_{rob})_{ij} \tag{28}$$

$$(P_{rob})_{ij} \geq 0 \text{ and} \tag{29}$$

$$\sum_{i=1}^{m} \sum_{j=1}^{n} (P_{rob})_{ij} = 1 \tag{30}$$

where $P_{prob}(W = w_i,\ K = k_J)$ is the probability mass function of W and K. Here, i is any value from zero to the maximum distance between the buses B and C, and j value is 1 to 4. The marginal probability mass function of W and K are shown in Equations (31)–(32).

$$P_{prob}(W = w_i) = \sum_j (P_{rob})_{ij} = P_{i1} + P_{i2} + P_{i3} + P_{i4} \tag{31}$$

$$P_{prob}(K = k_j) = \sum_i (P_{rob})_{ij} = P_{1j} + P_{1j} + P_{1j} + \ldots \tag{32}$$

5. Proposed Analytical Flow Chart for Determining the Frequency of Sag

5.1. Brief Explanation of the Flow Chart

1. Required data and assumptions are fed to the system.
2. Load flow analysis is performed to assess the pre-fault voltage with a fast and efficient load flow analysis technique [25].
3. A fault is created along the line, and its effect in terms of voltage is noted at the buses by using the Equations (12)–(27).
4. Then, the noted voltages are classified with respect to different ranges, and hence, a total number of associated sags of any given bus.
5. Step 3 is repeated for all the lines and different types of faults (SLGF, DLGF, LLF, LLLF, and LLLGF) of the tested system.
6. After that, the sag analysis is performed by using the bivariate joint discrete probability distribution method that uses a joint probability mass function that gives a clear idea about the probability of sag occurrence in different regions in a meshed network.

5.2. Flow Chart

The primary requirement of the study of sag assessment is to compute the probable frequency of sags per annum for all buses in the considered network, expressed with a specific limit of magnitude. For computing, the frequency of sags and the least magnitude of all the 3-phase voltages are taken into account. The procedure for obtaining the frequency of sags is shown in the flow chart in Figure 4. To obtain voltages before the fault magnitude, the backward–forward method of load-flow analysis is executed [25]. After that, the Z-bus is formed using the Z-bus building algorithm, which is used in creating the sequence impedance matrix and fault analysis in the network.

Then, the random fault location is selected in an arbitrarily chosen line. The sequence impedance matrix is formed to determine the post-fault voltage magnitudes in different phases of the buses. Fault analysis is performed by creating symmetrical and unsymmetrical faults for all the buses, and the residual magnitude of voltages is obtained along with the duration. Sag magnitude V_{Ψ}^{a} is determined for phase-a of bus Ψ from the list of voltage magnitudes obtained after the fault. If $V_L \leq V_{\Psi}^{a} \leq V_U$, then the corresponding upper and lower fault positions δ_U, δ_L for the line BC and the probable chances of fault occurrence between the lower fault position δ_L and the upper fault position δ_U are calculated. Then, the total number of sags is summated for the line BC. This procedure is performed for all types of unsymmetrical and symmetrical faults. The exact same process is carried out for the remaining lines of the considered network. Then, the total frequency of sags at any desired bus-Ψ is computed. After that, the results are processed for bivariate joint probability distribution to find the probability of sag occurrence in different frequency ranges with respect to the different types of faults.

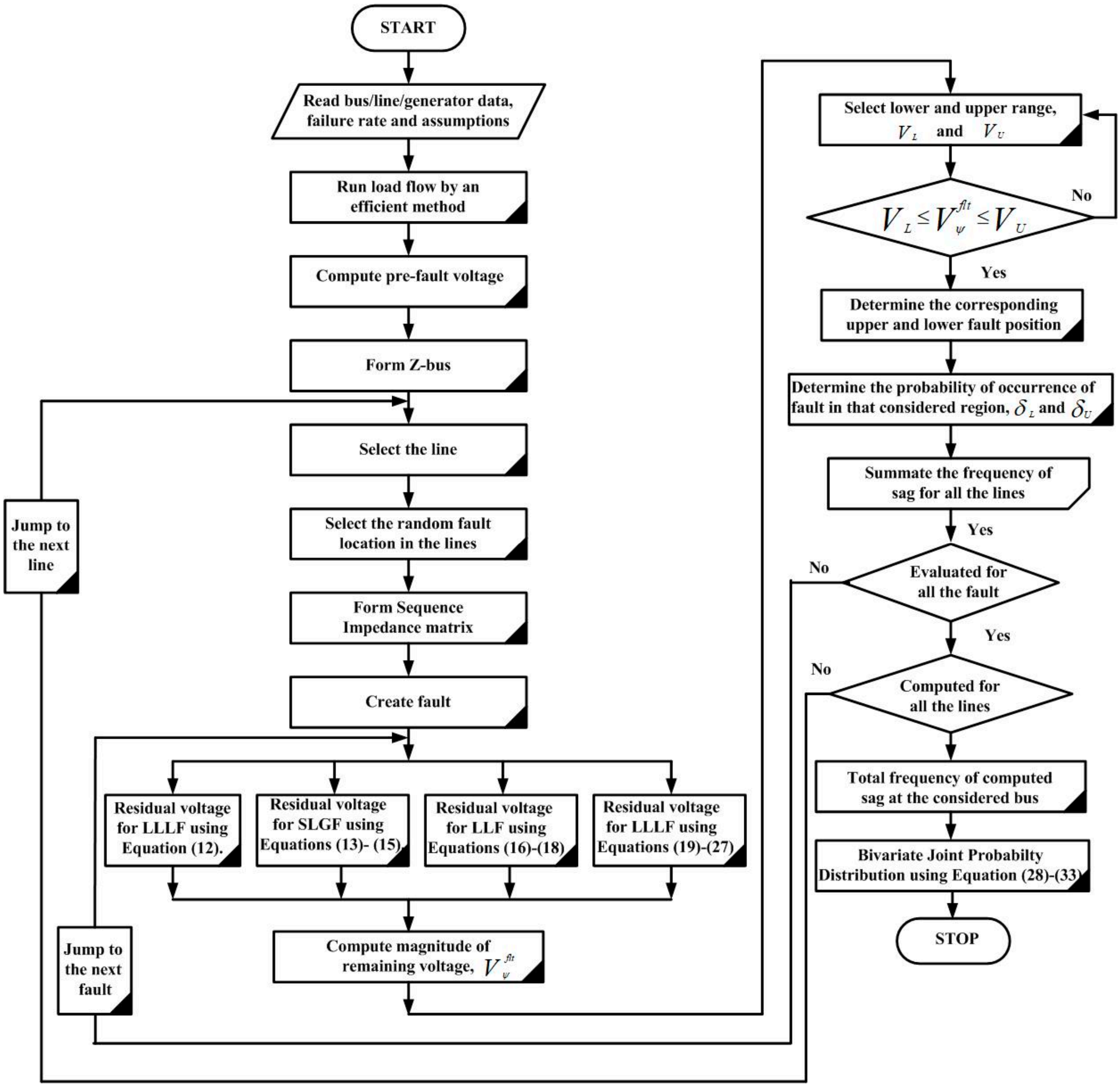

Figure 4. Suggested Methodology for evaluating frequency of sag incorporating efficient load flow technique [25] and bivariate probability distribution [24].

6. Case Study

Two networks (IEEE 39-bus reliability test system and an actual network of distribution system) have been taken for the study and the outcomes are discussed in Sections 6.1 and 6.2.

6.1. IEEE RTS-39 Bus Reliability Test System

The suggested analytical approach was tested on the IEEE 39-bus system, as shown in Figure 5. The test system data is given in [26]. The system contains 10 generators and 39 buses interlinked by 46 lines and 12 transformers. Various kinds of faults are taken into consideration to demonstrate the ability of the suggested mathematical approach to cope with symmetrical and unsymmetrical faults. Figure 6a shows the net frequency of sags of all the system buses for SLGF and DLGF.

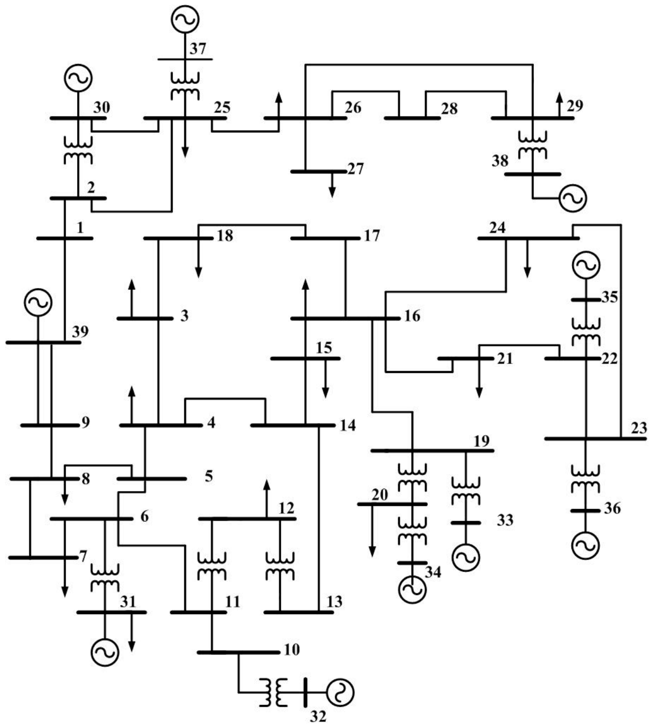

Figure 5. Single Line Diagram of the System IEEE 39-Bus Reliability Test.

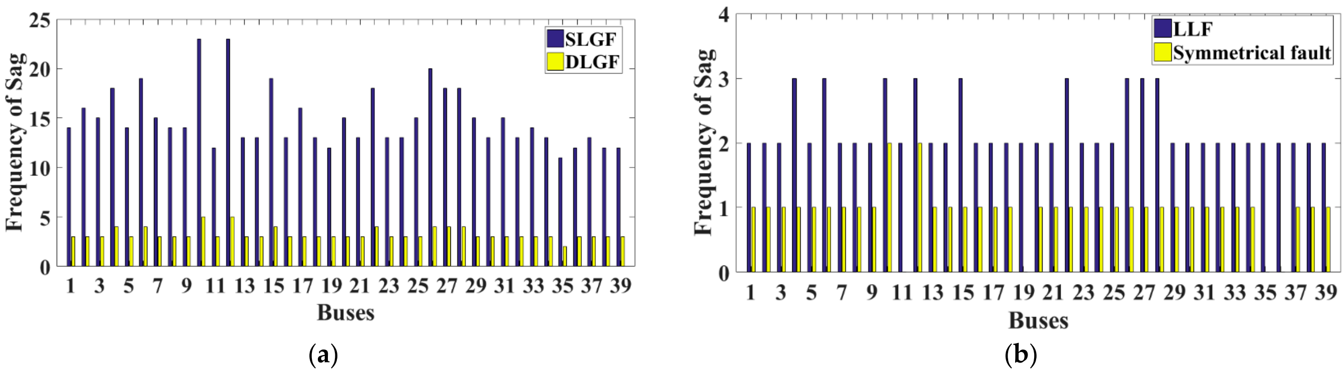

Figure 6. Voltage sags in all buses due to (**a**) SLGF and LLF; (**b**) DLGF and LLLF.

As a result of SLGF, the minimum frequency of sags occurred on bus 35, and the maximum frequency of sags occurred annually on buses 10 and 12. The associated frequencies were 11 and 23 sags per annum, respectively. Whereas the sags per annum due to DLGF was less than six identified on each bus, the maximum number of sags per annum due to DLGF was five, and it occurred on buses 10 and 12. In addition, the lowest frequency of sags per annum caused by DLGF was 2, which appeared on bus 35. The expected frequency of sags per year caused by LLF and the symmetrical fault is shown in Figure 6b. From Figure 6b, it is manifest that the sags per annum due to LLF was less than four identified on each bus, and a maximum number of sags per annum due to LLF was three, and it occurred on buses 4, 6, 10, 12, 15, 22, 26, 27, and 28.

Similarly, the highest frequency of sags per annum caused by three-phase faults was 1, which occurred almost in all buses except 11, 19, 35, and 36. By examining Figure 6, it can be identified that SLGF contributes to the maximum frequency of sags per annum, and it is a result of the most frequent occurrence of SLGF.

The comparative analysis of the proposed algorithm with respect to the existing algorithm is shown in Figure 7. Figure 7a shows the frequencies of sags due to the SLGF, and Figure 7b indicates the cumulative changes of voltage sags in the proposed and existing algorithms.

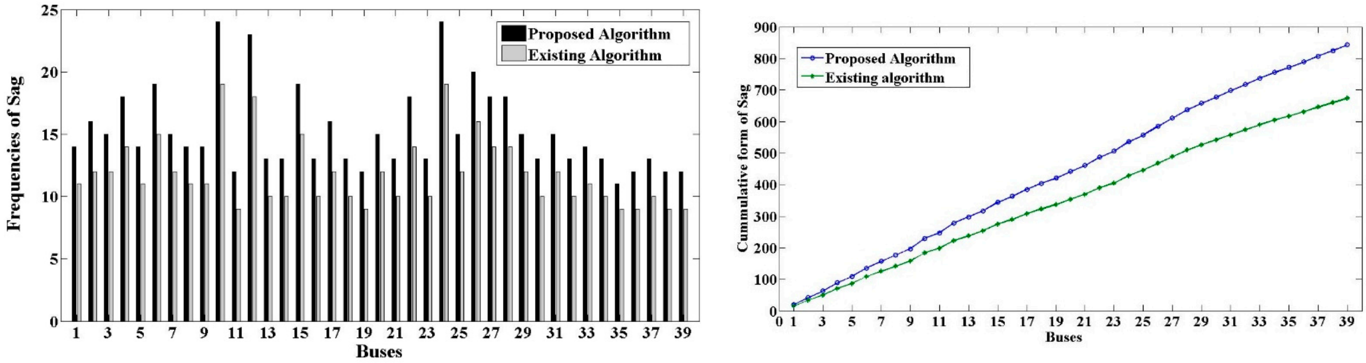

(**a**) (**b**)

Figure 7. Comparison of proposed and existing algorithm [3]; (**a**) Sags associated to SLGF; (**b**) Cumulative number of sags.

Figure 7 indicates that the frequency of sags is about 20% higher in the proposed algorithm.

The joint probability mass function of the sag range and different fault types is shown in Table 1. The values were obtained by using the Equations (28)–(32). Using that table, we can identify the probability of sag occurrence in different ranges with respect to the different faults. The analysis was performed on bus 15, but the table can similarly be obtained for the other buses.

Table 1. Joint probability mass function of sag range and fault type for bus 15.

Sag Range in p.u. (W)	Probabilities of Different Fault Type (K)				Total
	$P_{Prob}(LLLF)$	$P_{Prob}(SLGF)$	$P_{Prob}(LLF)$	$P_{Prob}(DLGF)$	
0.0–0.1	0.015152	0.060606	0.015152	0.015152	0.106061
0.1–0.2	0	0.045455	0.030303	0.015152	0.090909
0.2–0.3	0.015152	0.060606	0.015152	0.015152	0.106061
0.3–0.4	0	0.045455	0.030303	0.015152	0.090909
0.4–0.5	0	0.045455	0.030303	0.015152	0.090909
0.5–0.6	0.015152	0.060606	0.015152	0.015152	0.106061
0.6–0.7	0.015152	0.075758	0.030303	0.015152	0.136364
0.7–0.8	0.015152	0.075758	0.030303	0.015152	0.136364
0.8–0.9	0.015152	0.075758	0.030303	0.015152	0.136364
	$\sum P_{Prob}(LLLF) = 0.090909$	$\sum P_{Prob}(SLGF) = 0.545455$	$\sum P_{Prob}(LLF) = 0.227273$	$\sum P_{Prob}(DLGF) = 0.136364$	$\sum P_{Prob} = 1$

The probability of the occurrence of sag due to SLGF for the range of 0.8 to 0.9 p.u. was 0.075758.

Similarly, for the range of 0.0 to 0.1 p.u., the range was 0.060606. This analysis was performed for a time duration of 80 ms. The variation of the joint probability of sag due to SLGF for the different ranges of magnitude is shown in Figure 8.

From Figure 8, it is observed that for SLGF with a duration of 80 ms, the chances of sag occurrence are maximized in the range of 0.6 to 0.9 p.u. The variation is not linear due to the meshed system. The variation of sag magnitude with respect to the change of fault position for the duration of 80 ms is shown in Table 2. From Table 2, we can conclude that the highest magnitude of sag was 0.82 p.u. and the lowest was 0.07 p.u. The variation of voltage is not linear due to the meshed network.

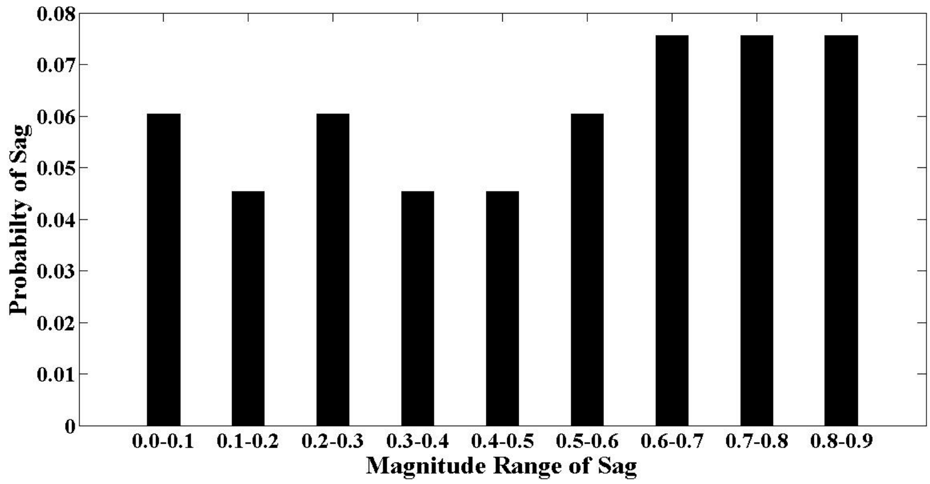

Figure 8. Joint probabilities of sag with respect to different magnitude ranges.

Table 2. Variation of sag magnitude concerning the change of fault position for the duration of 80 ms.

S.N	Fault Position Variation	Duration for SLGF in Sec	Variation of Magnitude of Sag
1.	0.1	0.008	0.07
2.	0.2	0.008	0.32
3.	0.3	0.008	0.5
4.	0.4	0.008	0.62
5.	0.5	0.008	0.69
6.	0.6	0.008	0.74
7.	0.7	0.008	0.78
8.	0.8	0.008	0.8
9.	0.9	0.008	0.81
10.	1	0.008	0.82
11.	1.1	0.008	0.82
12.	1.2	0.008	0.82
13.	1.3	0.008	0.81
14.	1.4	0.008	0.79
15.	1.5	0.008	0.77
16.	1.6	0.008	0.73
17.	1.7	0.008	0.67
18.	1.8	0.008	0.58
19.	1.9	0.008	0.44
20.	2	0.008	0.24
21.	2.1	0.008	0.07
22.	2.2	0.008	0.32
23.	2.3	0.008	0.5
24.	2.4	0.008	0.62
25.	2.5	0.008	0.69
26.	2.6	0.008	0.74
27.	2.7	0.008	0.77
28.	2.8	0.008	0.8
29.	2.9	0.008	0.81
30.	3	0.008	0.82

Table 2. *Cont.*

S.N	Fault Position Variation	Duration for SLGF in Sec	Variation of Magnitude of Sag
31.	3.1	0.008	0.82
32.	3.2	0.008	0.81
33.	3.3	0.008	0.8
34.	3.4	0.008	0.79
35.	3.5	0.008	0.76
36.	3.6	0.008	0.72

The three-dimensional ribbon plot of sag magnitude for different fault positions at a fixed duration of 80 ms is shown in Figure 9.

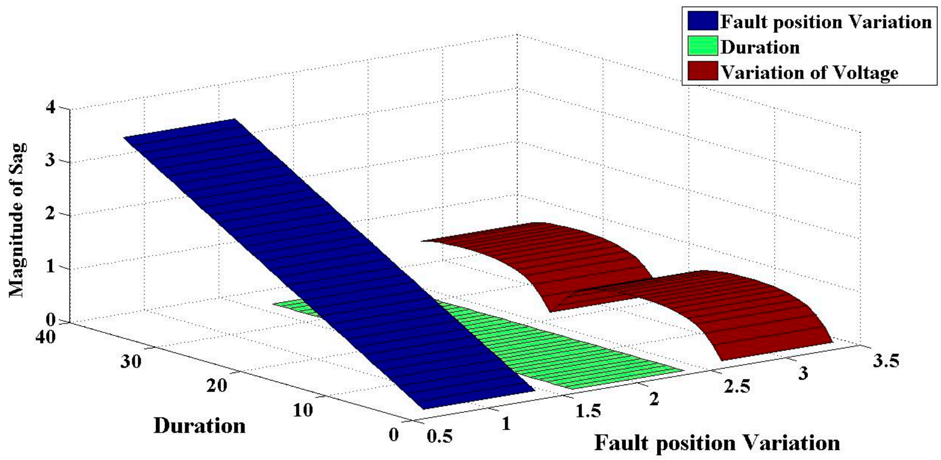

Figure 9. Three-dimensional ribbon plot of sag magnitude for different fault positions at a fixed duration of 80 ms.

From Table 2 and Figure 9, we can conclude that by the variation of fault position by 0.1 unit in a 100 km line, the sag magnitude also varies continuously. When the fault occurs close to bus 15, the voltage dip is greater, and the sag magnitude improves when the fault position is further away from bus 15. The variation of voltage is not linear due to the mesh system. The result may be linear for the radial distribution system.

6.2. Study of the Assessment of Sag in a Real Distribution Network

The suggested analytical approach was tested in a practical distribution system in the district of Haridwar in the state of Uttarakhand, India [27]. This network consists of 29 buses, 11 transformers, and 28 lines, as shown in Figure 10. The network has two 220 kV substations, i.e., Sidcul-220 and Roorkee-220, and seven 132 kV substations, i.e., Bhupatwala, Jwalapur, Ramnagar, Mangalore, Sidcul-132, Bhagwanpur, and Laksar. Moreover, the network has seven 33 kV buses, i.e., Ramnagar-33, Sidcul-33, Laksar-33, Mangalore-33, Bhagwanpur-33, Bhupatwala-33, and Jwalapur-33. The suggested approach was tested on a distribution network where the symmetrical and unsymmetrical faults are taken into account along the line and on the bus. The fault rates in the network are presented in Table 3 [18].

The assessment of voltage sag was performed on the considered real distribution network for every available bus. The frequency of sags concerning different magnitudes of duration for any usual bus 10 is shown in Figures 11 and 12.

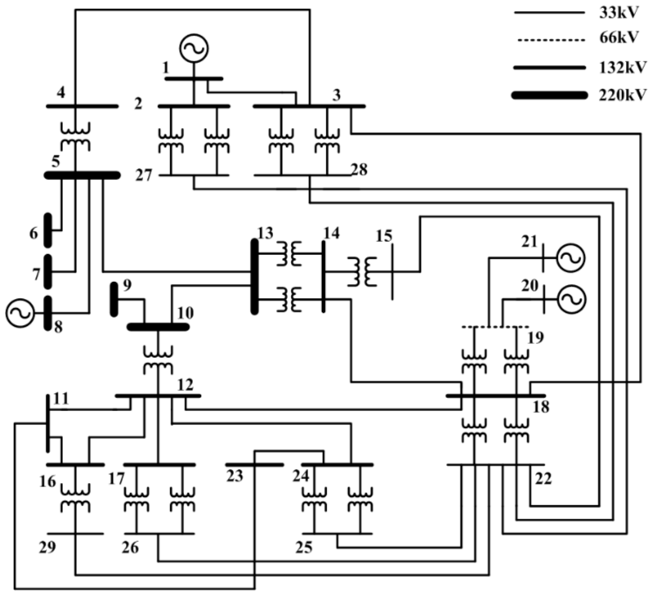

Figure 10. Distribution network of the district of Haridwar.

Table 3. Fault rate of the lines and buses.

Type of Fault	Fault Rate of Lines (Event/Year/100 km)	Fault Rate of Bus (Event/Year)
3Ph	0.100	0.003
SLGF	2.000	0.064
DLGF	0.300	0.008
LLF	0.125	0.004

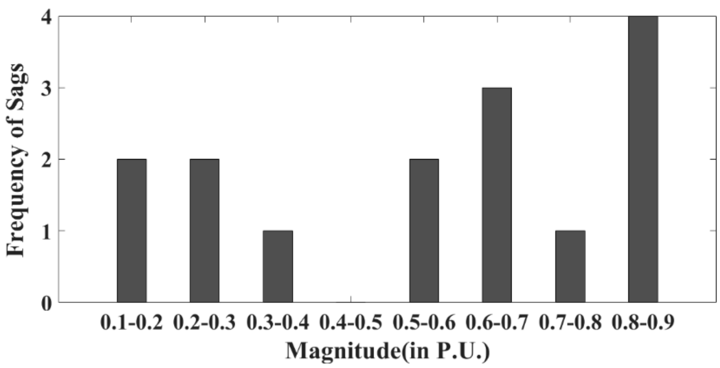

Figure 11. Assessment and comparison of voltage sag per year versus magnitude range of bus 10.

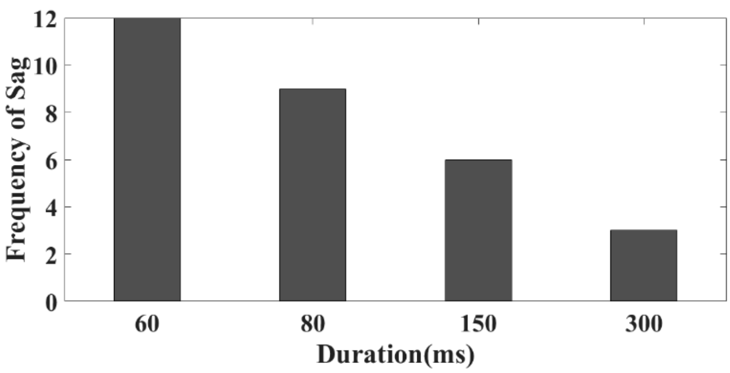

Figure 12. Frequency of sags versus duration on bus 10.

Figure 13 indicates the plot between the frequency of sags and the durations of the faults. From the graph, it is concluded that the maximum frequency of sag is associated with the lowest time duration, which was 60 ms. The frequency of sag concerning the duration and magnitude ranges are shown in Table 4 and Figure 13. From Table 4 and Figure 13, it is observed that the maximum frequency of sag associated with the highest magnitude range was 0.7–0.9 per unit and the lowest time duration was 60 ms.

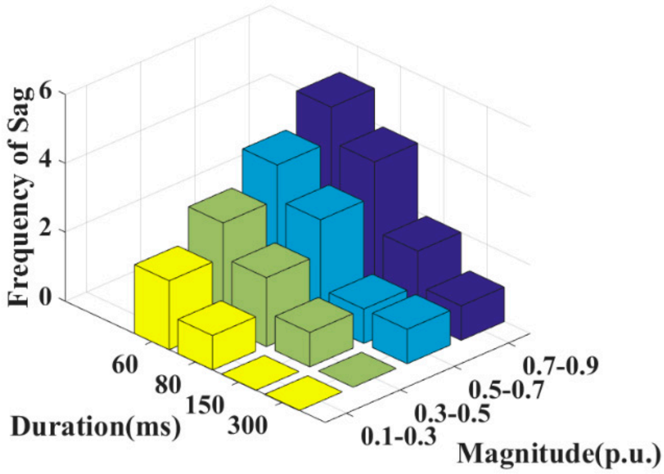

Figure 13. Sags per year for magnitude ranges and duration for bus 10.

Table 4. Frequency of sag with respect to duration and magnitude ranges for bus 10.

	Duration in Milliseconds (ms)			
Magnitude Ranges (p.u.)	**60 ms**	**80 ms**	**150 ms**	**300 ms**
0.1–0.3	1	1	0	0
0.3–0.5	2	1	1	0
0.5–0.7	4	3	2	1
0.7–0.9	5	4	3	2

The assessment of the frequency of sag concerning the magnitude of bus 15 is shown in Figure 14. Figure 15 indicates the plot between the frequency of sags concerning the durations of the faults. From the graph, it is concluded that the maximum frequency of sag is associated with the lowest time duration, which was 60 ms. The frequency of sag concerning the duration and magnitude ranges is shown in Table 5 and Figure 15.

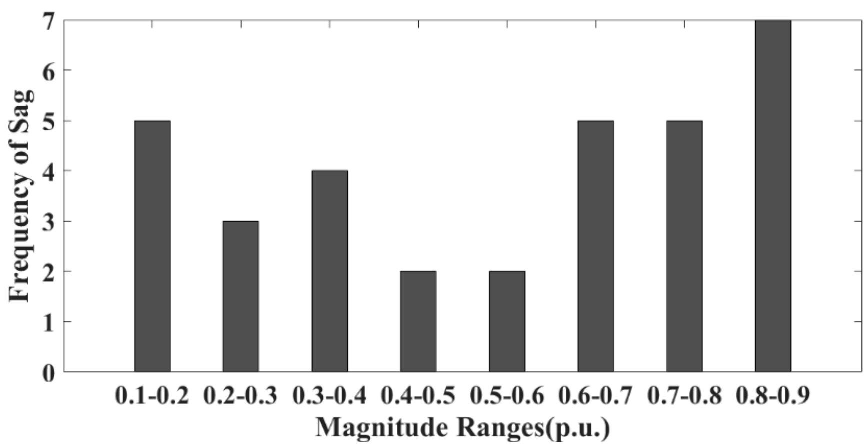

Figure 14. Voltage sag per year versus magnitude range at bus 15.

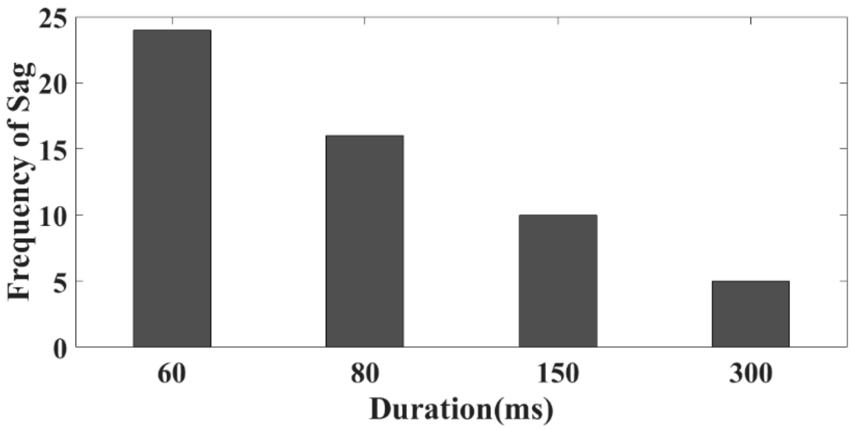

Figure 15. Sags per year for magnitude ranges and duration at bus 15.

Table 5. Frequency of sag for duration and magnitude ranges for bus 15.

	Duration (ms)			
Magnitude Ranges (p.u.)	**60 ms**	**80 ms**	**150 ms**	**300 ms**
0.1–0.3	3	2	1	0
0.3–0.5	5	3	2	1
0.5–0.7	7	4	3	2
0.7–0.9	9	7	4	2

From Figure 15 and Table 5, it is concluded that the frequency of sags is greater for the lower sag time duration and less for the comparatively more extended period. Furthermore, it is identified that the frequency of deep sags is less than that of shallow sags. A fault causes deep sags in the lower magnitude voltage part of the network, which affects only the neighboring consumer. In contrast, the shallow sags occur due to the faults in the transmission lines, and their consequences spread over a broader part of the distribution system. The maximum frequency of sags was 66 annually, and the minimum was 18 for bus 15 and bus 10, respectively. The sag frequency of the four randomly chosen buses, 10, 15, 23, and 29, is presented in Table 6 and Figure 16.

Table 6. Frequency of sag versus magnitude in some observed buses.

	Buses			
Magnitude Range	**Bus 10**	**Bus 15**	**Bus 23**	**Bus 29**
0.0–0.1	0	7	3	6
0.1–0.2	1	6	2	5
0.2–0.3	1	7	2	6
0.3–0.4	2	6	0	4
0.4–0.5	1	6	2	5
0.5–0.6	2	7	3	6
0.6–0.7	4	9	4	7
0.7–0.8	3	9	2	6
0.8–0.9	4	9	6	7

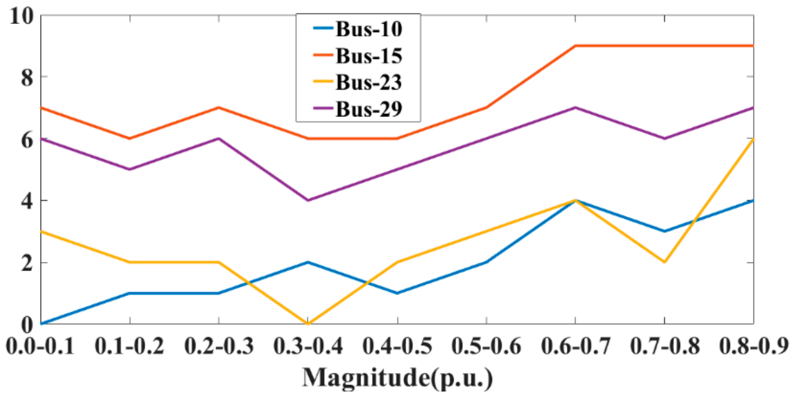

Figure 16. Sags per year for buses 10, 15, 23, and 29 with respect to magnitude.

The frequency of sag concerning different types of faults for the same randomly chosen buses, 10, 15, 23, and 29, is shown in Figure 17. It is identified that the maximum and minimum frequencies of sag were due to a single line to ground fault and a three-phase fault, respectively.

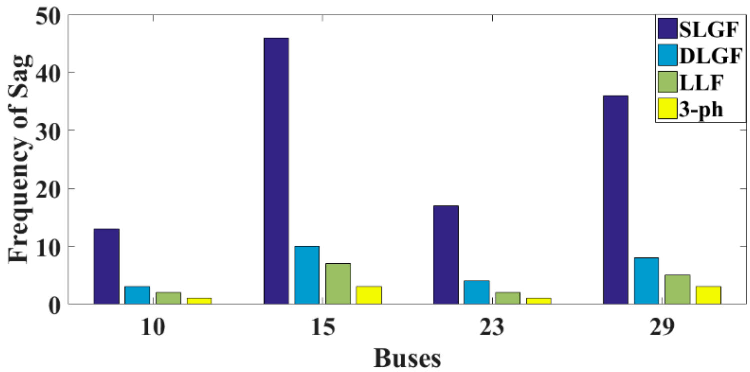

Figure 17. Sags per year for buses 10, 15, 23, and 29 with respect to different types of faults.

7. Conclusions and Future Scope

In the presented study, residual voltages caused by faults along the line and on the buses were obtained and inspected. Fault impedance was incorporated into the entire analysis. The work is extended with a comparison to reference [3]. In that paper, fault impedance was not considered and was followed by the existing typical load flow analysis technique. In the presented article, fault impedance is introduced, due to which more voltage sags occur, which is treated better so that the industrial consumer will be prepared for this type of contingency. In this article, a fast and efficient load flow analysis technique [25] is used that produces fast results. Computational performance is also enhanced. The sag analysis was performed by using the bivariate joint discrete probability distribution method that uses a joint probability mass function that gives a clear idea about the probability of sag occurrence in a meshed network.

The suggested approach was tested in India's IEEE 39-bus system and an existing distribution system. This proposed approach computes the probable sag frequency resulting from symmetrical and unsymmetrical faults. The assessment result was compared with an existing analytical method. An assessment of higher sag frequency is beneficial for industrial customers so that alternate voltage sag mitigation arrangements can be introduced for smooth industrial operation. The disadvantage of this algorithm is that it is limited to the evaluation of sag as well as associated weak areas only, but it does not provide a clear idea regarding the voltage sag source location, except for the created fault position. The future research can be extended to voltage sag source location areas. Also, this voltage sag study can be extended in the field of economic and macroeconomic analyses [28].

Author Contributions: Conception, design of the study, acquisition of data, and analysis and interpretation of data were carried out by J.P. and drafting the manuscript was performed by N.P. All authors have read and agreed to the published version of the manuscript.

Funding: This research received no external funding.

Data Availability Statement: Not applicable.

Conflicts of Interest: The authors report no conflict of interest. The authors alone are responsible for the content and writing of this article.

References

1. Dugan, R.C. *Electrical Power System Quality*, 2nd ed.; McGraw-Hill: New York, NY, USA, 1996; pp. 43–109.
2. Bollen, M.H.J. *Understanding Power Quality Problems, Voltage Sags and Interruptions*; IEEE Press: Piscataway, NJ, USA, 2000; pp. 139–248.
3. Goswami, A.K.; Gupta, C.P.; Singh, G.K. An analytical approach for assessment of voltage sags. *J. Electr. Power Energy Syst.* **2009**, *31*, 418–426. [CrossRef]
4. Serrano-Fontova, A.; Casals Torrens, P.; Bosch, R. Power quality disturbances assessment during unintentional islanding scenarios. A contribution to voltage sag studies. *Energies* **2019**, *12*, 3198. [CrossRef]
5. Han, Y.; Feng, Y.; Yang, P.; Xu, L.; Xu, Y.; Blaabjerg, F. Cause, Classification of Voltage Sag, and Voltage Sag Emulators and Applications: A Comprehensive Overview. *IEEE Access* **2020**, *8*, 1922–1934. [CrossRef]
6. Deng, Y.; Liu, X.; Jia, R.; Huang, Q.; Xiao, G.; Wang, P. Sag Source Location and Type Recognition via Attention-based Independently Recurrent Neural Network. *J. Mod. Power Syst. Clean Energy* **2021**, *9*, 1018–1031. [CrossRef]
7. Yalman, Y.; Uyanık, T.; Atlı, İ.; Tan, A.; Bayındır, K.Ç.; Karal, Ö.; Golestan, S.; Guerrero, J.M. Prediction of Voltage Sag Relative Location with Data-Driven Algorithms in Distribution Grid. *Energies* **2022**, *15*, 6641. [CrossRef]
8. Mohammadi, Y.; Salarpour, A.; Leborgne, R.C. Comprehensive strategy for classification of voltage sags source location using optimal feature selection applied to support vector machine and ensemble techniques. *Int. J. Electr. Power Energy Syst.* **2021**, *124*, 106363. [CrossRef]
9. Arias-Guzmán, S.; Ruiz-Guzman, O.A.; Garcia-Arias, L.F.; Jaramillo-Gonzales, M.; Cardona-Orozco, P.D.; Ustariz-Farfan, A.J.; Cano-Plata, E.A.; Salazar-Jimenez, A.F. Analysis of Voltage Sag Severity Case Study in an Industrial Circuit. *IEEE Trans. Ind. Appl.* **2017**, *53*, 15–21. [CrossRef]
10. Begum, M.T.A.; Alam, M.R.; Muttaqi, K.M. Analytical expressions for characterising voltage dips and phase-angle jumps in electricity networks. *IET Gener. Transm. Distrib.* **2019**, *13*, 116–126. [CrossRef]
11. Alam, M.R.; Muttaqi, K.M.; Bouzerdoum, A. Characterizing Voltage Sags and Swells Using Three-Phase Voltage Ellipse Parameters. *IEEE Trans. Ind. Appl.* **2015**, *51*, 2780–2790. [CrossRef]
12. Hao, C.; Jin, J. Clustering Analysis of Voltage Sag Events Based on Waveform Matching. *Processes* **2022**, *10*, 1337. [CrossRef]
13. Otcenasova, A.; Bodnar, R.; Regula, M.; Hoger, M.; Repak, M. Methodology for determination of the number of equipment malfunctions due to voltage sags. *Energies* **2017**, *10*, 401. [CrossRef]
14. Milanović, J.V.; Gupta, C.P. Probabilistic assessment of financial losses due to interruptions and voltage sags—Part II: Practical implementation. *IEEE Trans. Power Deliv.* **2006**, *21*, 925–932, 2006. [CrossRef]
15. Motoki, É.M.; da Silveira, P.M.; Pereira, N.B.; de Souza, P.V.G. Cost of Industrial Process Shutdowns Due to Voltage Sag and Short Interruption. *Energies* **2021**, *14*, 2874. [CrossRef]
16. Behera, C.; Reddy, G.H.; Chakrapani, P.; Goswami, A.K.; Gupta, C.P.; Singh, G.K. Assessment of equipment trip probability due to voltage sags based on fuzzy possibility distribution function. *IEEE Access* **2018**, *6*, 76889–76899. [CrossRef]
17. Dos Santos, A.; Rosa, T.; de Barros, M.T.C. Stochastic characterization of voltage sag occurrence based on field data. *IEEE Trans. Power Deliv.* **2018**, *34*, 496–504. [CrossRef]
18. Park, C.H.; Jang, G. Stochastic estimation of voltage sags in a large meshed network. *IEEE Trans. Power Deliv.* **2007**, *22*, 1655–1664. [CrossRef]
19. Khatri, N.; Kumar, V.; Bansal, R.C.; Joshi, R.R. Stochastic evaluation of voltage sag in power system network considering effect of photovoltaic generation. *Int. Trans. Electr. Energy Syst.* **2019**, *29*, 2773. [CrossRef]
20. dos Santos, A.; de Barros, M.C. Voltage sag prediction for network planning. *Electr. Power Syst. Res.* **2016**, *140*, 976–983. [CrossRef]
21. Mitra, R.; Goswami, A.K.; Tiwari, P.K. Voltage sag assessment using type-2 fuzzy system considering uncertainties in distribution system. *IET Gener. Transm. Distrib.* **2017**, *11*, 1409–1419. [CrossRef]
22. Sadat, H. *Power System Analysis*; McGraw-Hill: New York, NY, USA, 2002; pp. 335–442.
23. Behera, C.; Banik, A.; Goswami, A.K. A novel approach for voltage sag representation in a chemical industry: A case study. *Eng. Rep.* **2020**, *2*, 12198. [CrossRef]
24. Devore, J.L. *Probability and Statistics for Engineering and the Science*, 8th ed.; Brooks/Cole: Boston, MA, USA; Cengage Learning: Boston, MA, USA, 2012; pp. 193–230.
25. Ghatak, U.; Mukherjee, V. A fast and efficient load flow technique for unbalanced distribution system. *Int. J. Electr. Power Energy Syst.* **2017**, *84*, 99–110. [CrossRef]

26. IEEE 39-Bus Test Case. Available online: http://icseg.iti.illinois.edu/ieee-39-bus-system (accessed on 21 October 2020).
27. UPCL Network Details. Available online: www.upcl.org (accessed on 21 October 2020).
28. Küfeoğlu, S.; Lehtonen, M. Macroeconomic assessment of voltage sags. *Sustainability* **2016**, *8*, 1304. [CrossRef]